The Astrophysical Journal, 765:104 (11pp), 2013 March 10 doi:10.1088/0004-637X/765/2/104

CANDELS: THE PROGENITORS OF COMPACT QUIESCENT GALAXIES AT $z \sim 2$

Guillermo Barro[1], S. M. Faber[1], Pablo G. Pérez-González[2,3], David C. Koo[1], Christina C. Williams[4], Dale D. Kocevski[1], Jonathan R. Trump[1], Mark Mozena[1], Elizabeth McGrath[1], Arjen van der Wel[5], Stijn Wuyts[6], Eric F. Bell[7], Darren J. Croton[8], Ceverino Daniel[9], Avishai Dekel[9], M. L. N. Ashby[10], Edmond Cheung[1], Henry C. Ferguson[11], Adriano Fontana[12], Jerome Fang[1], Mauro Giavalisco[4], Norman A. Grogin[11], Yicheng Guo[1,4], Nimish P. Hathi[13], Philip F. Hopkins[14], Kuang-Han Huang[11], Anton M. Koekemoer[11], Jeyhan S. Kartaltepe[15], Kyoung-Soo Lee[16], Jeffrey A. Newman[17], Lauren A. Porter[18], Joel R. Primack[18], Russell E. Ryan[11], David Rosario[6], Rachel S. Somerville[19], Mara Salvato[6], and Li-Ting Hsu[6]

[1] UCO/Lick Observatory and Department of Astronomy and Astrophysics, University of California, Santa Cruz, CA 95064, USA
[2] Departamento de Astrofìsica, Facultad de CC Fìsicas, Universidad Complutense de Madrid, F. CC. Físicas, E-28040 Madrid, Spain
[3] Associate Astronomer at Steward Observatory, 933 N. Cherry Street, University of Arizona, Tucson, AZ 85721, USA
[4] Astronomy Department, University of Massachusetts, 710 N. Pleasant Street, Amherst, MA 01003, USA
[5] Max-Planck-Institut für Astronomie, Königstuhl 17, D-69117 Heidelberg, Germany
[6] Max-Planck-Institut für extraterrestrische Physik, Postfach 1312, Giessenbachstr., D-85741 Garching, Germany
[7] Department of Astronomy, University of Michigan, 500 Church St., Ann Arbor, MI 48109, USA
[8] Centre for Astrophysics and Supercomputing, Swinburne University of Technology, P.O. Box 218, Hawthorn, VIC 3122, Australia
[9] Racah Institute of Physics, The Hebrew University, Jerusalem 91904, Israel
[10] Harvard-Smithsonian Center for Astrophysics, 60 Garden St., Cambridge, MA 02138, USA
[11] Space Telescope Science Institute, 3700 San Martin Drive, Baltimore, MD 21218, USA
[12] INAF Osservatorio Astronomico di Roma, Via Frascati 33, I-00040 Monteporzio, Rome, Italy
[13] Observatories of the Carnegie Institution of Washington, Pasadena, CA 91101, USA
[14] Department of Astronomy, University of California Berkeley, Berkeley, CA 94720, USA
[15] National Optical Astronomy Observatory, 950 N. Cherry Ave., Tucson, AZ 85719, USA
[16] Department of Physics, Purdue University, 525 Northwestern Avenue, West Lafayette, USA
[17] Department of Physics and Astronomy, University of Pittsburgh, 3941 O'Hara Street, Pittsburgh, PA 15260, USA
[18] Santa Cruz Institute for Particle Physics, University of California, Santa Cruz, CA 95064, USA
[19] Department of Physics and Astronomy, Rutgers, The State University of New Jersey, Piscataway, NJ 08854, USA
Received 2012 June 15; accepted 2013 January 18; published 2013 February 21

ABSTRACT

We combine high-resolution *Hubble Space Telescope*/WFC3 images with multi-wavelength photometry to track the evolution of structure and activity of massive ($M_\star > 10^{10}\ M_\odot$) galaxies at redshifts $z = 1.4$–3 in two fields of the Cosmic Assembly Near-infrared Deep Extragalactic Legacy Survey. We detect compact, star-forming galaxies (cSFGs) whose number densities, masses, sizes, and star formation rates (SFRs) qualify them as likely progenitors of compact, quiescent, massive galaxies (cQGs) at $z = 1.5$–3. At $z \gtrsim 2$, cSFGs present SFR = 100–200 $M_\odot\ \mathrm{yr}^{-1}$, yet their specific star formation rates (sSFR $\sim 10^{-9}\ \mathrm{yr}^{-1}$) are typically half that of other massive SFGs at the same epoch, and host X-ray luminous active galactic nuclei (AGNs) 30 times (∼30%) more frequently. These properties suggest that cSFGs are formed by gas-rich processes (mergers or disk-instabilities) that induce a compact starburst and feed an AGN, which, in turn, quench the star formation on dynamical timescales (few 10^8 yr). The cSFGs are continuously being formed at $z = 2$–3 and fade to cQGs down to $z \sim 1.5$. After this epoch, cSFGs are rare, thereby truncating the formation of new cQGs. Meanwhile, down to $z = 1$, existing cQGs continue to enlarge to match local QGs in size, while less-gas-rich mergers and other secular mechanisms shepherd (larger) SFGs as later arrivals to the red sequence. In summary, we propose two evolutionary tracks of QG formation: an early ($z \gtrsim 2$), formation path of rapidly quenched cSFGs fading into cQGs that later enlarge within the quiescent phase, and a late-arrival ($z \lesssim 2$) path in which larger SFGs form extended QGs without passing through a compact state.

Key words: galaxies: high-redshift – galaxies: photometry – galaxies: starburst

Online-only material: color figures

1. INTRODUCTION

Nearby galaxies come in two flavors (Kauffmann et al. 2003; Baldry et al. 2004): red quiescent galaxies (QGs) with old stellar populations, and blue young star-forming galaxies (SFGs). This color bimodality seems to be already in place at $z \sim 2$–3 (Faber et al. 2007; Ilbert et al. 2010; Brammer et al. 2011), presenting also strong correlations with mass, size, and morphology: SFGs are typically larger than QGs of the same mass (Williams et al. 2010; Wuyts et al. 2011b) and disk-like, whereas QGs are typically spheroids characterized by concentrated light profiles (Bell et al. 2012).

A major surprise has been the discovery of smaller sizes for massive QGs at $z \sim 2$. These compact QGs (cQGs), also colloquially known as "red nuggets" (Damjanov et al. 2009), are ∼5 times smaller than local, equal-mass analogs (Trujillo et al. 2007; Buitrago et al. 2008; Toft et al. 2007; Saracco et al. 2010; Cassata et al. 2011; Szomoru et al. 2011). In contrast, most of the massive SFGs at $z \gtrsim 2$ have relatively large disks (Kriek et al. 2009a; Förster Schreiber et al. 2009). Therefore, since there is an evolutionary connection between these two populations (Buitrago et al. 2013; Patel et al. 2012), the structural differences present a puzzle. If we adopt the view that galaxy mass growth is accompanied by size growth, as suggested by the mass–size

relation, then, in order to form compact QGs from larger SFGs, three changes are required: a significant shrinkage in radius, an increase in mass concentration, and a rapid truncation of the star formation.

Proposed mechanisms to create compact spheroids from star-forming progenitors generally involve violent, dynamical processes (Naab et al. 2007; Oser et al. 2010), such as gas-rich mergers (e.g., Hopkins et al. 2006, 2008) or dynamical instabilities fed by cold streams (Kereš et al. 2005; Dekel et al. 2009a; Ceverino et al. 2010). Recent hydrodynamical simulations of mergers have reproduced some of the observed properties of cQGs (Wuyts et al. 2010), if high amounts of cold gas, as observed by Tacconi et al. (2010) or Daddi et al. (2010a), are adopted.

If cQGs are so formed, we expect to see a co-existing population of compact SFGs and recently quenched galaxies at $z \gtrsim 2$. Recent works demonstrate the existence of such populations (Cava et al. 2010; Wuyts et al. 2011b; Whitaker et al. 2012a; Kaviraj et al. 2013), but a direct evolutionary link has not yet been clearly established.

This paper illustrates a connection between compact star-forming galaxies (cSFGs) and QGs at high-z. We combine the deepest photometric data from the optical to the far-IR from the Great Observatories Origins Deep Survey (GOODS; Giavalisco et al. 2004), the UKIDSS Ultra Deep Survey (UDS), the Cosmic Assembly Near-infrared Deep Extragalactic Legacy Survey (CANDELS; Grogin et al. 2011; Koekemoer et al. 2011), FIDEL,[20] and SpUDS[21] to estimate stellar masses, star formation rates (SFRs), and sizes for massive, high-z galaxies. By analyzing the global evolution in the space defined by these parameters, we suggest two paths for QG formation from $z \sim 3$ to $z \sim 1$.

We adopt a flat cosmology with $\Omega_M = 0.3$, $\Omega_\Lambda = 0.7$, and $H_0 = 70$ km s^{-1} Mpc^{-1}.

2. DATA DESCRIPTION

This paper is based on a sample of massive galaxies built from the *Hubble Space Telescope* (*HST*)/WFC3 F160W (H-band) selected catalog ($H_{5\sigma}$(AB) = 27 mag) for the GOODS-S and UDS fields of CANDELS. Consistent, multi-wavelength photometry (U-band to 8 μm) was measured using TFIT (Laidler et al. 2006), implemented as described by Guo et al. (2011) and A. Galametz et al. (2013, in preparation). Photometric redshifts were computed using EAZY (Brammer et al. 2008) and yielded errors of $\Delta z/(1+z) = 3\%$ and 6% at $z > 1.5$ in GOODS-S and UDS, respectively. This data set is partially described in Wuyts et al. (2011b); for full details, see T. Dahlen et al. (2013, in preparation). Stellar masses were derived using FAST (Kriek et al. 2009b) and based on a grid of Bruzual & Charlot (2003) models that assume a Chabrier (2003) IMF, solar metallicity, exponentially declining star formation histories, and the Calzetti et al. (2000) dust extinction law.

SFRs were computed by combining IR and rest-frame UV (uncorrected for extinction) luminosities (Kennicutt 1998 and Bell et al. 2005) and adopting a Chabrier (2003) initial mass function (IMF; see Barro et al. 2011 for more details): $\mathrm{SFR_{UV+IR}} = 1.09 \times 10^{-10}(L_{\mathrm{IR}} + 3.3L_{2800})$. Total IR luminosities ($L_{\mathrm{IR}} \equiv L$[8–1000 μm]) were derived from Chary & Elbaz (2001) templates fitting MIPS 24 μm fluxes, applying a *Herschel*-based re-calibration (Elbaz et al. 2011). For galaxies undetected by MIPS below a 2σ level (20 μJy) and for galaxies detected in the X-rays, SFRs come from rest-frame UV luminosities that are corrected for extinction as derived from spectral energy distribution (SED) fits (Wuyts et al. 2011a). $L_{\mathrm{X}} \equiv L_{2-8\,\mathrm{kev}}$ were computed for the sources in the *Chandra* 4Ms image in GOODS-S (Xue et al. 2011) and the *XMM* 50–100 ks survey in UDS (Ueda et al. 2008). Due to the shallower detection limits in the IR and X-ray surveys of UDS, the detection fractions are computed only on GOODS-S data.

Circularized, effective (half-light) radii, $r_e \equiv a_{\mathrm{eff}}\sqrt{(b/a)}$ (a_{eff} is the half-light radii on the major axis), and Sèrsic indices were measured from *HST*/WFC3 H images using GALFIT (Peng et al. 2002) and point spread functions (PSFs) created and processed to replicate the conditions of the observed data (van der Wel et al. 2011; van der Wel et al. 2013).

3. SAMPLE SELECTION

We selected a sample of galaxies at $1.4 < z < 3.0$ with $M_\star > 10^{10}\,M_\odot$, above which our sample is >90% complete up to the highest redshifts (Wuyts et al. 2011b; Newman et al. 2012). Compact galaxies were based on H-band sizes; quiescent galaxies (QGs) and SFGs were separated by a specific SFR (sSFR) of $10^{-0.5}$ Gyr^{-1} (see Figure 1). Although somewhat arbitrary, the value does not strongly affect the results, since the sSFR bimodality is clearly detected up to $z = 3$.

Figure 1 also shows a mass–size diagram for our sample. In agreement with recent results, we find that SFGs and QGs follow significantly different mass–size relations (Williams et al. 2010; Wuyts et al. 2011b). With this in mind, we select compact galaxies as those following the observed trend in the mass–size relation for QGs at $z > 1.5$. The threshold is defined as $\log(M/r_e^\alpha) = 10.3\ M_\odot$ kpc$^{-\alpha}$, with $\alpha = 1.5$. The slope is roughly consistent with those given by Newman et al. (2012) for QGs at similar redshifts ($\alpha^{-1} = 0.59$–0.69). The zero point is chosen to include the majority of QGs with minimum contamination from SFGs. For $\alpha = 1.5$, M/r_e^α (hereafter $\Sigma_{1.5}$) lies between the surface density, $\Sigma = M/r_e^2$, and M/r_e, both of which follow strong correlations with color and SFR up to high redshifts (e.g., Franx et al. 2008; Patel et al. 2012).

Figure 2 shows the evolution of sSFRs versus $\Sigma_{1.5}$ for massive galaxies from $z = 3.0$ down to $z = 0.5$. In this diagram, our size–mass–SFR selection is completely orthogonal. Although our analysis focuses on $z > 1.4$, two panels at lower redshifts are shown to illustrate the extrapolated evolutionary trends. We find that the number of QGs (above the line) increases rapidly since $z = 3$, starting from very small number densities, $n \sim 10^{-5}$ Mpc^{-3}, at $z \sim 2.8$. Among these, the number of compact QGs (cQG; $\Sigma_{1.5} > 10.3$) builds up first, and only at $z < 1.8$ we do start finding a sizable number of extended QGs. This suggests that the bulk of these galaxies are assembled at late times by both continuous migration (quenching) of non-compact SFGs (bottom-left region) and size growth of cQGs. As a result of this growth, the population of cQGs disappears by $z <\sim 1$. Simultaneously, we identify a population of compact SFGs (cSFGs) whose number density decreases steadily with time since $z = 3.0$, being almost completely absent at $z < 1.4$. The number of cSFGs makes up less than 20% of all massive SFGs, but they present similar number densities as cQGs down to $z \sim 2$, suggesting an evolutionary link between the two populations.

[20] http://irsa.ipac.caltech.edu/data/SPITZER/FIDEL/
[21] http://irsa.ipac.caltech.edu/data/SPITZER/SpUDS/

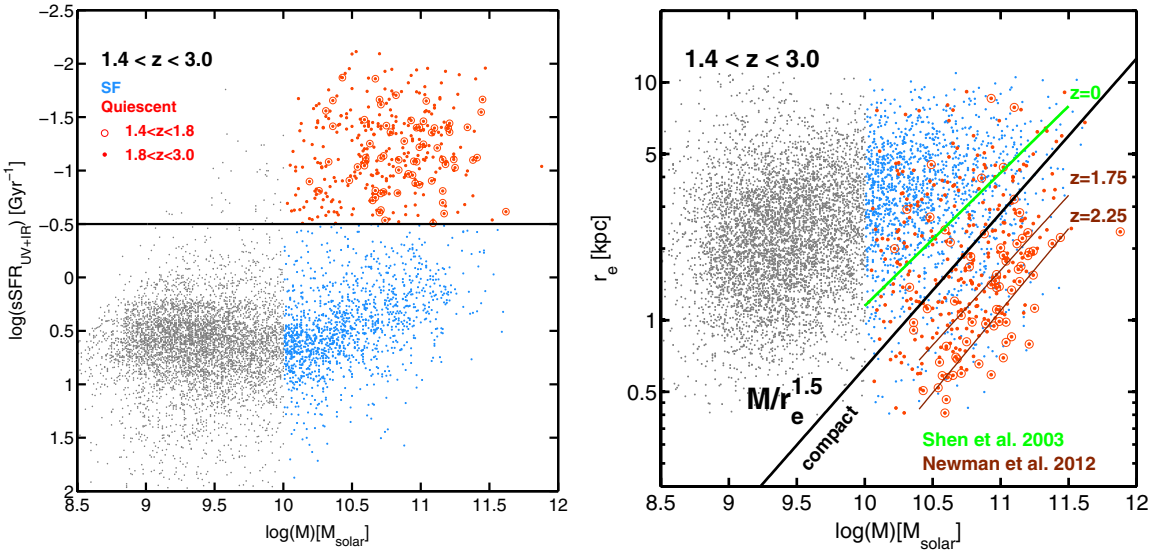

Figure 1. Left panel: specific SFR as a function of the stellar mass for galaxies at $1.4 < z < 3.0$. The solid black line defines our threshold, $\log(\mathrm{sSFR}) = -0.5$, to select QGs (red in both panels) and SFGs (blue) above $M_\star > 10^{10}\,M_\odot$. The gray dots show galaxies with stellar masses below the mass selection limit. Right panel: stellar mass–size relation at $1.4 < z < 3.0$. The solid black line defines our selection criterion for compact galaxies, $M/r_e^{1.5} \equiv \Sigma_{1.5} = 10.3\,M_\odot\ \mathrm{kpc}^{-1.5}$. The green line shows the local mass–size relation for elliptical galaxies (Shen et al. 2003). The thin brown lines are the mass–size relations for QGs found at $z = 1.75$ and $z = 2.25$ by Newman et al. (2012).

(A color version of this figure is available in the online journal.)

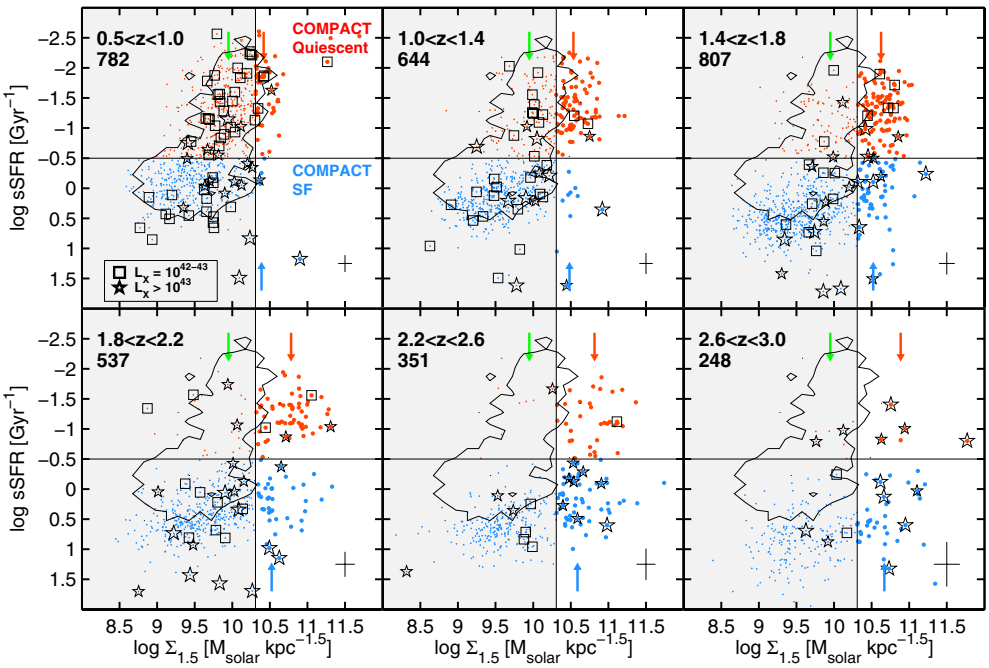

Figure 2. Evolution of the sSFR vs. $\Sigma_{1.5} \equiv M/r_e^{1.5}$ correlation at $0.5 < z < 3.0$ for galaxies above $M_\star > 10^{10}\,M_\odot$. The redshift bins are chosen to probe similar comoving volumes. The solid lines and colored dots depict the selection thresholds for SFGs (blue) and QGs (red) and compact (white region) and non-compact (shaded region), as defined in Figure 1. The open markers depict sources detected in the X-rays at different luminosities: squares have $10^{42}\,\mathrm{erg\,s^{-1}} < L_X < 10^{43}\ \mathrm{erg\ s^{-1}}$; small (large) stars have $L_X > 10^{43}$ (10^{44}; i.e., QSO) erg s^{-1}. The blue and red arrows indicate the median $\Sigma_{1.5}$ of cSFGs and cQGs, respectively. The green arrows approximate the local mass–size relation (Shen et al. 2003). The black contour shows the sSFR–$\Sigma_{1.5}$ distribution for 90% of the galaxies at $0.5 < z < 1.0$. The lower right error bars for $\Sigma_{1.5}$ and the sSFR include uncertainties in: half-light radii, stellar masses, rest-frame luminosities (derived by perturbing photometric redshifts within the 1σ errors), and the average *rms* of the comparison between UV-corrected and (UV+IR)-based SFR estimates.

(A color version of this figure is available in the online journal.)

4. CO-EVOLUTION OF COMPACT SFGs AND QGs

An evolutionary sequence where cSFGs are the progenitors of cQGs at lower redshifts is supported by the fact that cSFGs first appear before cQGs at high redshift ($z = 2.6$–3.0) and then disappear before them at low redshift ($z = 1.0$–1.4), implying that evolution is from blue through red rather than vice versa. Therefore, if we assume that cSFGs would see their star formation quenched and fade at roughly constant $\Sigma_{1.5}$, these could rapidly populate the compact quiescent region in timescales of ∼500 Myr (approx. one of our redshift intervals).

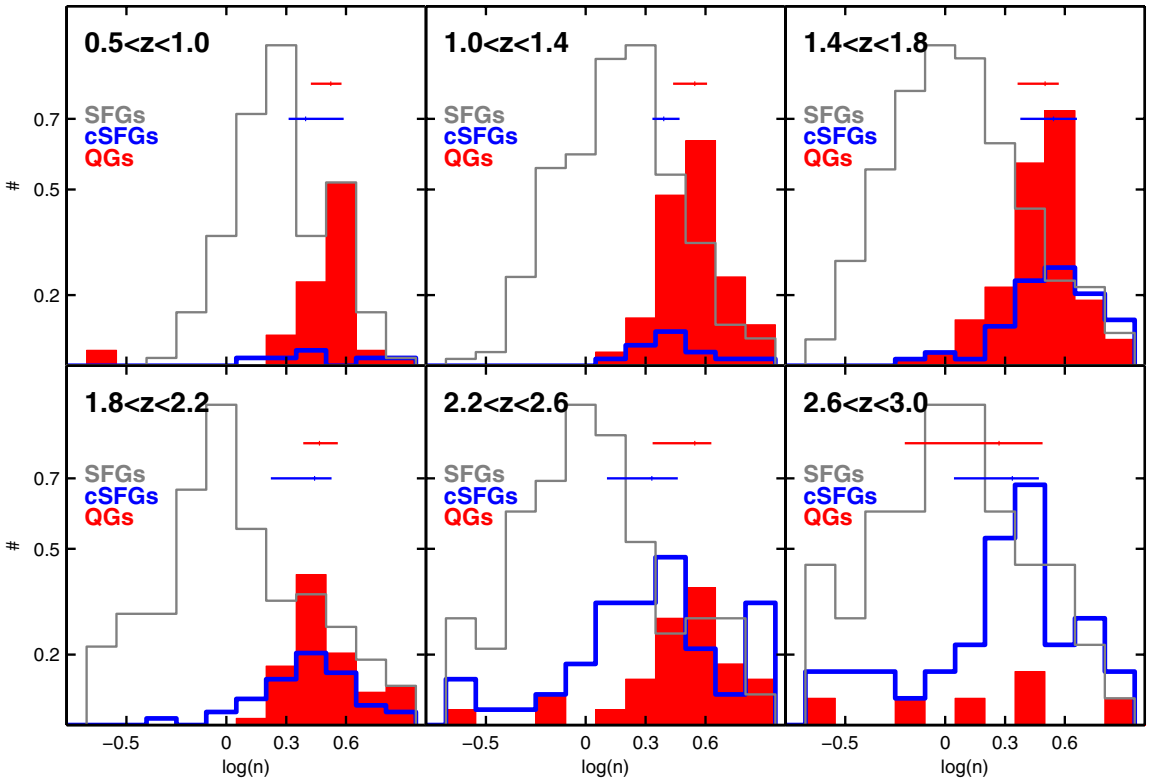

Figure 3. Distribution of the Sérsic index values for SFGs (gray), cSFGs (blue), and QGs (red) at $0.5 < z < 3.0$. The bulk of SFGs exhibit a larger scatter and a peak around $n \sim 1$, while cSFGs and QGs present similar higher values with the average ranging between $n = 2.5$–3.5 and $n = 3$–4, respectively.
(A color version of this figure is available in the online journal.)

A more detailed analysis of the sizes of cSFGs and cQGs shows that, indeed, both populations have median effective radii slightly smaller than 1 kpc (similar to the findings in van der Wel et al. 2011; Szomoru et al. 2011). The median $\Sigma_{1.5}$ of cQGs (red arrows in Figure 2) decrease by 0.25 dex (i.e., increase their radii by a factor of ∼2) from $z = 3.0$ to $z = 1.4$, in agreement with previous results on the size evolution of QGs (Cassata et al. 2011), whereas cSFGs present smaller values of $\Sigma_{1.5}$ (blue arrows) by ∼0.2 dex, and a weaker evolution with time. However, cSFGs migrating to the red sequence are expected to slowly increase their masses with time, thus moving to higher values of $\Sigma_{1.5}$ at lower redshifts. Given their median sSFR, the typical mass-doubling times for cSFGs range from 0.6 to 1 Gyr. This is enough to account for the observed difference in $\Sigma_{1.5}$ between cSFGs and cQGs, provided that the newly formed stars do not significantly increase the galaxy radii.

Figure 3 shows the distribution of Sérsic index values for the same galaxies and redshift bins depicted in Figure 2. Both cQGs and cSFGs present similar surface brightness profiles, which are best represented by large Sérsic indices. The median values range from $n = 3$–4 for cQGs to $n = 2.5$–3.5 for cSFGs. This means that both populations are preferentially concentrated, in contrast with non-compact SFGs ($n \sim 1$). As discussed in Wuyts et al. (2011b; see also Szomoru et al. 2011; Bell et al. 2012), a strong correlation between quiescence (lower sSFR) and high-Sérsic values is still present up to $z \gtrsim 2$. However, this is not strictly true for SFGs, which typically exhibit a larger scatter, minimized for main-sequence (Elbaz et al. 2011) galaxies with $n \sim 1$, and a reversal toward higher Sérsic indices for galaxies with enhanced SFRs and, as shown in Figure 3, galaxies with more compact structures (higher $\Sigma_{1.5}$). The median axis ratios of cSFGs, $b/a \sim 0.65$, are also consistent with spheroidal morphologies. However, cQGs present slightly smaller axis ratios, $b/a \sim 0.54$, suggesting that some of these are small flattened disks (van der Wel et al. 2011; Bruce et al. 2012). This feature might be explained if cQGs developed an extended component surrounding the compact core, perhaps via minor mergers (Naab et al. 2009; Bezanson et al. 2009) or regrowth of a remnant disk that survived the major merger (Governato et al. 2009; Hopkins et al. 2009a). These mechanisms will continue to growth these galaxies in size, eventually depopulating the compact region.

Turning back to the possibility of cSFGs fading into cQGs, we find that although the majority (∼60%–80%) of cSFGs are clearly detected at 24 μm, yielding SFR = 100–200 $M_{\odot}$ yr^{-1}, they also present suppressed sSFRs compared to the bulk of SFGs. Figure 4 shows the distribution of sSFRs at $1.4 < z < 3.0$ corrected for the redshift dependence of the main-sequence zero point (e.g., Karim et al. 2011; Whitaker et al. 2012b) using the $z = 1.6$ redshift bin as reference. The median value of the sSFR for cSFGs is ∼0.24 dex lower than that for non-compact SFGs, suggesting that, on average, the star formation in the compact evolutionary stage has started to quench. There are, however, a few cSFGs at the high sSFR end of the distribution, indicating that this is a heterogeneous population which includes some galaxies at the peak of their star formation, as shown also in Wuyts et al. (2011b). The low number of galaxies with such high SFRs however may be an indication of short duty cycles in the formation of cSFGs (see Sections 5 and 6 for further discussion).

Finally, we find an increasing fraction of cSFGs hosting X-ray detected active galactic nuclei (AGNs) at $z > 2$ (open markers in Figure 2). This result also supports the quenching scenario, since AGN seems to be connected with quenching

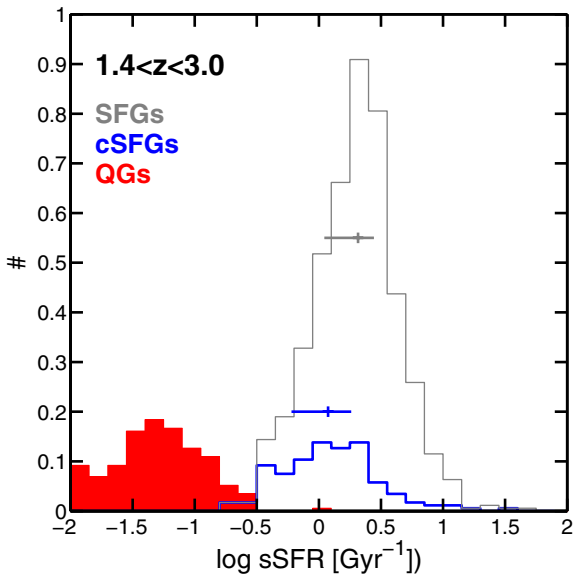

Figure 4. Distribution of the sSFRs for galaxies at $1.4 < z < 3.0$ corrected for the redshift evolution in the zero point of the main sequence using the value at $z = 1.6$ as reference. cSFGs (blue) present sSFRs that are on average ∼0.24 dex lower than the whole SFG population (gray), which may indicate that star formation on these galaxies started to quench.

(A color version of this figure is available in the online journal.)

of the star formation on timescales of a few hundred Myr (Di Matteo et al. 2005; Hopkins et al. 2006). In particular, a high-luminosity quasar phase ($L_X > 10^{44}$ erg s^{-1}), associated with high black hole accretion rates, would be particularly efficient at removing the available gas, thus stopping the star formation. Using data from the deepest X-ray survey in GOODS-S, we find that cSFGs host X-ray luminous AGNs 30× (∼30%) more frequently than non-compact (<1%) (but massive) SFGs at $z \gtrsim 2.2$. This implies that, at these epochs, the majority of luminous ($L_X > 10^{43}$ erg s^{-1}) AGNs are found preferentially in compact hosts, as opposed to lower redshifts, where AGNs are more frequent in non-compact galaxies (Kocevski et al. 2012). Interestingly, (the few) cQGs at $z \sim 2.8$ also show a high fraction of X-ray detections (>70%), strengthening the idea that AGNs might play an important role on the quenching of star formation (see also Olsen et al. 2013).

4.1. X-Ray Detected cSFGs

We note that the estimates of the star formation activity and structural properties for X-ray detected sources can be biased by the presence of an AGN. This section describes the additional test performed to quantify the impact of such effects. We note, however, that the population of cSFGs remains clearly detected (see, e.g., Figure 2), even if we remove the AGNs from the sample.

X-ray sources with a strong AGN continuum emission can outshine the light of their host (Type I AGNs; typically $L_X > 10^{43.5}$ erg s^{-1}), thereby hampering the estimation of photometric redshifts and stellar parameters from SED modeling, if this contribution is not properly taken into account. In our sample of cSFGs at $z \gtrsim 2$, more than 60% of the X-ray sources have spectroscopic redshifts, and for the remaining galaxies, we used the photometric redshifts of Xue et al. (2011), computed from a set of templates that include both stellar and AGN components. In addition, we also fitted the SEDs of these galaxies with AGN templates, following the procedures of Salvato et al. (2009, 2011) to quantify the level of contamination by Type I AGNs. We find that only four spectroscopically confirmed sources are best fit with a pure AGN template, while the remaining 10 are fit with either a galaxy template or a hybrid, where a Type II AGN is used. In this case, the contamination on the SED is not significant. For all X-ray detected sources, we use the UV-corrected SFRs instead of the IR-based ones, as these may be contaminated by AGN-heated dust. For the four sources that are best fit with Type I AGN templates, the contamination of the AGN to the stellar SED can bias the estimate of the stellar mass up to ∼0.2 dex (Marchesini et al. 2010; Santini et al. 2012). However, their hosts would still be classified as cSFGs, even after correcting for this factor.

Point-source contamination by a bright AGN component could also bias the structural parameters of otherwise larger galaxies toward more compact morphologies (Simmons & Urry 2008; Pierce et al. 2010). We verified that these galaxies are genuinely compact by comparing to the (light profile independent) sizes estimated with SExtractor (Bertin & Arnouts 1996). The typical Kron (1980) radius for the smallest galaxies ranges between 3 to 4 pixels (1.5–2 kpc), which, for an average Sérsic index of ∼2.5, implies an effective radii slightly above 1 kpc (Graham et al. 2005), a value in good agreement with the GALFIT estimates. Only if these galaxies make an unusual population of galaxies with extremely flat light profiles ($n < 1$), we would expect a slight overestimation of their sizes by ∼0.15 dex. Visual inspection of the X-ray detected cSFGs also shows no evidence of bright point sources within extended galaxies or significant distortions that could bias the measurements of the structural parameters. In fact, these galaxies present smooth profiles consistent with spheroidal morphologies, as found among the rest of the cSFGs. Our visual inspection results are also consistent with the results of the CANDELS visual classifications (M. Mozena et al., in preparation). Here, two or more unbiased (unaware of their AGN nature) classifiers inspect each galaxy to assess their disk-like or spheroidal appearances and identify possible disturbances.

5. NUMBER DENSITY OF COMPACT GALAXIES

Figure 5 shows the number density evolution of massive cQGs and cSFGs. The best fit (red line) to the increasing number density of QGs can be parameterized as $n = a + b(1 + z)$, with $a = 1.75 \times 10^{-4}$ and $b = -6.75 \times 10^{-4}$. Assuming that all cQGs at a given redshift z' come from cSFGs, we can estimate how many of the latter we should observe at $z > z'$. To do so, we propose a simple evolutionary model that assigns to all SFGs an arbitrary lifetime for their current burst of star formation, $\Delta t_{\rm burst}$, after which they will become quiescent. The number of cQGs at a given time would be

$$n_{\rm QG}(t + \Delta t_{\rm burst}) = n_{\rm QG}(t) + n_{\rm SFG}(t). \quad (1)$$

We explore $\Delta t_{\rm burst}$ values from 0.3 Gyr to 1.0 Gyr, similar to the typical e-folding times expected for SFGs at these redshifts (Wuyts et al. 2011a). The observed number density of cSFGs is broadly consistent with the model prediction for a median value of $\Delta t_{\rm burst} \sim 800$ Myr.

This simple model assumes, that at every step, $\Delta t_{\rm burst}$, enough cSFGs are being formed by some mechanism(s), restoring the ones that turned into cQGs. Plausible mechanisms to reduce the size of massive (larger) SFGs are gas-rich dissipational processes, such as mergers or dynamical instabilities. These can produce compact, starbursting remnants that would likely

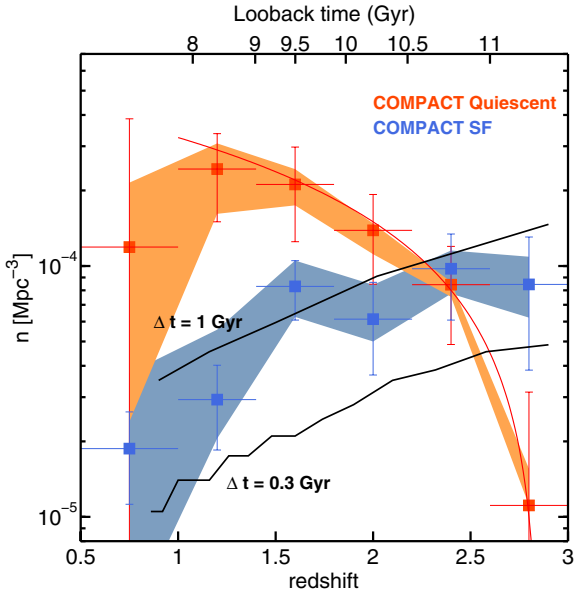

Figure 5. Number density evolution of massive, $M_\star > 10^{10}\,M_\odot$, cQGs (red), and cSFGs (blue) vs. redshift. The solid red line is the best fit to the number density of cQGs. The solid black lines depict the evolution of the number of cSFGs required to match the observed increasing density of cQGs, assuming that the former have lifetimes of $\Delta t_{\rm burst} = 0.3$–1 Gyr. The error bars were computed by bootstrapping the sSFR and $\Sigma_{1.5}$ uncertainties along with terms for small number statistics and field-to-field differences. The shaded regions encompass the observed number densities when the selection thresholds in sSFR and $\Sigma_{1.5}$ are modified by ± 0.2 dex.

(A color version of this figure is available in the online journal.)

quench in a short period of time (Springel et al. 2005; Hopkins et al. 2006; Dekel et al. 2009b). Without relying on mergers being the main or sole driver of this transformation, we can make a quantitative estimate of the number of cSFGs assembled by this mechanism by using typical numbers for major mergers at these redshifts. Considering pair fractions of roughly 10% (Williams et al. 2011), merger timescales of 1 Gyr (Lotz et al. 2011) and a density of massive galaxies of $\lesssim 10^{-3}$ Mpc^{-3} (Pérez-González et al. 2008), we obtain an assembly rate for new cSFGs via mergers of $\Delta n_{\rm cSFG} \sim 10^{-4}$ Gyr^{-1}, which is roughly consistent with the observed densities for the predicted $\Delta t_{\rm burst}$.

In this model, the significant drop in numbers of cSFGs by $z < 1.4$ implies that the formation mechanism(s) become quickly inefficient at lower redshifts, thereby truncating the formation of new cSFGs and thus cQGs. The decline on the efficiency of the dissipational processes may follow the decline in the amount of available gas in galaxies (Geach et al. 2011) and dark matter halos (e.g., Croton 2009). Detailed comparisons to cosmological models will allow tests of this hypothesis and provide a more rigorous modeling of the number density evolution (L. A. Porter et al., in preparation; D. Ceverino et al., in preparation). Some of the key questions to be explored with simulations: What are the possible evolutionary paths for massive SFGs on the mass–size plane? What are the mechanisms that would trigger their transition from extended (disk-like) to compact (spheroid-like) structures? Simulations predict that both gas-rich major mergers (Hopkins et al. 2009a; Wuyts et al. 2010) and disk instabilities (Dekel et al. 2009b; Ceverino et al. 2010) can form cSFGs by stochastically transforming only a fraction of the larger population of normal SFGs. This process effectively shifts those (larger) galaxies into a steeper mass–size relation (Covington et al. 2008, 2011). Alternatively, very early phases of star formation could be dominated by strongly dissipational, but efficiently *cold flow* fed (Kereš et al. 2005; Dekel et al. 2009a; Oser et al. 2010), processes. In this case, the size of the majority of SFGs would remain small, moving horizontally in the mass–size diagram as they grow in stellar mass. A critical issue for the models is whether the compact, star-forming phase is the norm or the exception.

6. SUMMARY AND DISCUSSION

Using the deepest data spanning from the X-ray-to-MIR, along with high-resolution imaging from CANDELS in GOODS-S and UDS, we analyze stellar masses, SFRs, and sizes of a sample of massive ($M_\star > 10^{10}\,M_\odot$) galaxies at $z = 1.4$–3.0 to identify a population of cSFGs with similar structural properties as cQGs at $z \gtrsim 2$. The cSFG population is already in place at $z \sim 3$, but it completely disappears by $z < 1.4$. A corresponding increase in the number of cQGs during the same time period suggests an evolutionary link between them.

A simple duty-cycle argument, involving quenching of the star formation activity on timescales of $\Delta t = 0.3$–1 Gyr, is able to broadly reproduce the evolution of the density of new QGs formed since $z = 3$ in terms of fading cSFGs. Under this assumption, we also need to invoke a replenishment mechanism to form new cSFG via gas-rich dissipational processes (major mergers or dynamical instabilities), that then become quickly inefficient at $z \lesssim 1.5$, as the flow of cold gas from progressively more massive halos decreases with time (e.g., Croton 2009).

The early phases of cSFG formation would then be associated with disturbed morphologies, either tidal tails or multiple clumps, enhanced star formation, and the rapid assembly of a compact stellar component (Hopkins et al. 2009a; Ceverino et al. 2010). Simultaneously, the compact phase can also trigger an AGN, and sometimes a short-lived quasar, followed by a rapid decline of the star formation in ~1 Gyr (Springel et al. 2005; Hopkins et al. 2008; Ciotti et al. 2009). The observed properties of cSFGs are consistent with intermediate to late stages of this process. They present spheroidal morphology with no visible traces of mergers, and although they have high (dusty) SFRs of a few 100 $M_\odot$ yr^{-1}, their sSFRs are on average half that of the bulk of massive SFGs suggesting that they already started quench. Simultaneously, ~30% of them host luminous ($L_X > 10^{43}$ erg s^{-1}) X-ray detected AGNs at $z > 2$, which might play a relevant role in the quenching of star formation.

Our observations connect two recent results at $z \gtrsim 2$: the discovery of a population of compact, high-Sérsic ($n \gtrsim 2$) galaxies with enhanced star formation activity (Wuyts et al. 2011b), and the finding of an increasing fraction of small, post-starburst galaxies that have recently arrived on the red sequence (Whitaker et al. 2012a). Together, the results indicate that early phases of galaxy quenching happen preferentially in compact spheroids. Nevertheless, a substantial fraction of the quiescent population is formed at lower redshifts (Bell et al. 2004; Faber et al. 2007), and observations suggest that many of the transitioning (*green valley*) galaxies have extended structures and disk morphologies (Mendez et al. 2011). Therefore, in the general context of galaxy quenching, our result suggests that the truncation of star formation follows different evolutionary paths on a Σ–sSFR plane diagram (illustrated in Figure 6), each one dominating at different epochs, and characterized by structurally different (compact versus extended) populations.

In the *early track*, $z = 3.0$–2.0, the number of passive galaxies builds up rapidly upon quenching of spheroid-like cSFGs with high mass densities ($\Sigma_{1.5} > 10.5$). This population constitutes

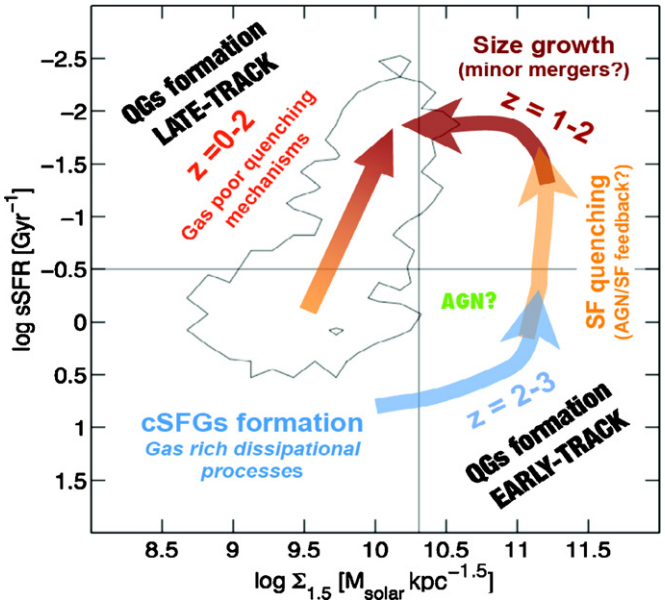

Figure 6. Schematic view of a two path (early/late track) formation scenario for QGs. The arrows indicate the time evolution and quenching sequence, the black contour shows the galaxy distribution at low redshift. On the early track, a small fraction of the massive SFGs at $z = 2$–3 evolve (e.g., through gas-rich dissipational processes) to a compact starbursting remnant. Then, the star formation is quenched in $\lesssim$1 Gyr (by gas exhaustion or stellar and AGN feedback), and galaxies fade into cQGs. Once in the red sequence, cQGs grow envelopes, over longer timescales, depopulating the compact region by $z \sim 1$. Simultaneously, at $z \lesssim 2$, other mechanisms have already started to populate the red-sequence with normal-sized, non-compact QGs (formed by, e.g., secular processes, halo quenching, or gas-poor mergers).

(A color version of this figure is available in the online journal.)

the first generation of red sequence galaxies and consists almost exclusively of *compact* QGs. Along this track, cQGs are only actively forming down to $z \sim 2$, because, at lower redshifts, the formation mechanisms for new cSFGs (and consequently new cQGs) quickly become inefficient. If cSFGs are the remnants of gas-rich dissipational processes, a possible explanation for the truncation of this track could be the decline with time in galaxy gas content (and gas accretion), thereby reducing the efficiency of these events to produce compact spheroids (Springel & Hernquist 2005; Robertson et al. 2006). In that case, the track would be most efficient at $z \gtrsim 2$, where SFGs are found to have larger gas reservoirs (Tacconi et al. 2010; Genzel et al. 2010; Daddi et al. 2010a), that allow some of them to sustain high-efficiency star formation modes (Daddi et al. 2010b; Rodighiero et al. 2011; Sargent et al. 2012; Kartaltepe et al. 2012). A rapidly grown central cusp will eventually quench star formation on timescales of ∼1 Gyr. This quenching is most likely due to a combination of gas consumption and highly efficient star formation or AGN feedback (Di Matteo et al. 2005; Hopkins et al. 2008). If, indeed, rapid flow of cold gas is the main driver of the *early track*, it can also be the triggering mechanism for rapidly growing (luminous) AGNs in cSFGs. If so, a link is provided between the peak epoch of cSFGs formation and quasar activity (Aird et al. 2010). These results also suggest the early build up of the σ–M_{BH} (black hole) correlation (e.g., Ferrarese & Merritt 2000), which has been shown to be in place at least up to $z \sim 2$ (Cisternas et al. 2011; Mullaney et al. 2012).

In the *late track*, at $z < 2$, cSFGs are not formed in large numbers and, therefore, new quiescent galaxies must form upon quenching of more *extended* SFGs with lower mass densities ($\Sigma_{1.5} < 10.5$). As a result, the quiescent population at these redshifts constitute a mixture of (1) compact spheroids (Cassata et al. 2011; Szomoru et al. 2012), formed along the *early track*, and that are continuously growing inside-out (van Dokkum et al. 2010; Patel et al. 2012), e.g., by minor mergers (Naab et al. 2009; Hilz et al. 2012), and thereby becoming progressively less compact; (2) extended galaxies, including a significant population of passive disks (van der Wel et al. 2011; Bruce et al. 2012). The fading of star-forming disks appears to be a key transitioning stage responsible for many of the new additions to the red sequence at low redshifts (Scarlata et al. 2007; Ilbert et al. 2010; Mendez et al. 2011), particularly at the low mass end (Bundy et al. 2010). This disk fading suggests that the importance of strongly dissipational processes diminish with time, perhaps due to the decreasing amount gas in the halo reservoir. As a consequence, other quenching mechanisms that partially preserve the structural properties of the galaxies become more important. Some possibilities include the build up of a large central density (bulge) that could stop star formation either by stabilizing the disk, preventing further fragmentation of the gas (morphological quenching; Martig et al. 2009) or by secular processes, causing gas to migrate from the disk to the center (Kormendy & Kennicutt 2004); stellar and AGN feedback removing the gas after virial shock heating shuts down accretion from the halo (halo quenching; Birnboim & Dekel 2003; Cattaneo et al. 2006; Gabor & Davé 2012); less gas-rich mergers or dynamical instabilities, where a new disk component can be rebuilt before quenching completes (Hopkins et al. 2009b; Governato et al. 2009; Naab & Trujillo 2006).

Regardless of the mechanisms, recent works indicate that quiescence correlates best with Σ, velocity dispersion or Sérsic index than with stellar mass or color (Bell et al. 2012; Wake et al. 2012; Bezanson et al. 2012), suggesting that quenching of the star formation, at any redshift, involves some transformation of the internal structure of the galaxy toward more concentrated mass profiles. In fact, the build up of a central mass has been shown to be tightly connected with quenching in the local universe (Bell 2008; Masters et al. 2010) as well as at higher redshifts (Franx et al. 2008; Cheung et al. 2012). In this regard, both the *early* and *late* tracks on the Σ–sSFR plane might be the result of a similar central mass build up taking place under different gas abundances or gas feeding modes.

Support for Program number HST-GO-12060 was provided by NASA through a grant from the Space Telescope Science Institute, which is operated by the Association of Universities for Research in Astronomy, Incorporated, under NASA contract NAS5-26555. G.B. acknowledges support from NSF grant AST-08-08133. P.G.P.-G. acknowledges support from grant AYA2009-07723-E.

APPENDIX A

SELECTION OF COMPACT GALAXIES IN THE MASS–SIZE DIAGRAM

In this Appendix, we address the robustness of the selection criteria for compact galaxies. As described in Section 2, compact galaxies are selected using a pseudo surface density threshold, $\Sigma_{1.5} \equiv \log(M/r_e^{\alpha}) = 10.3\ M_{\odot}\ \mathrm{kpc}^{-\alpha}$, with $\alpha = 1.5$. The inverse value of α is the slope of the mass–size relation, described as $r_e = \gamma M^{\alpha^{-1}}$, where γ is the mass-normalized radius or zero point of the mass–size relation. The values of α and $\Sigma_{1.5}$ are chosen to include the bulk of the quiescent population at $z > 1.5$. However, Figure 2 illustrates how this criterion also identifies

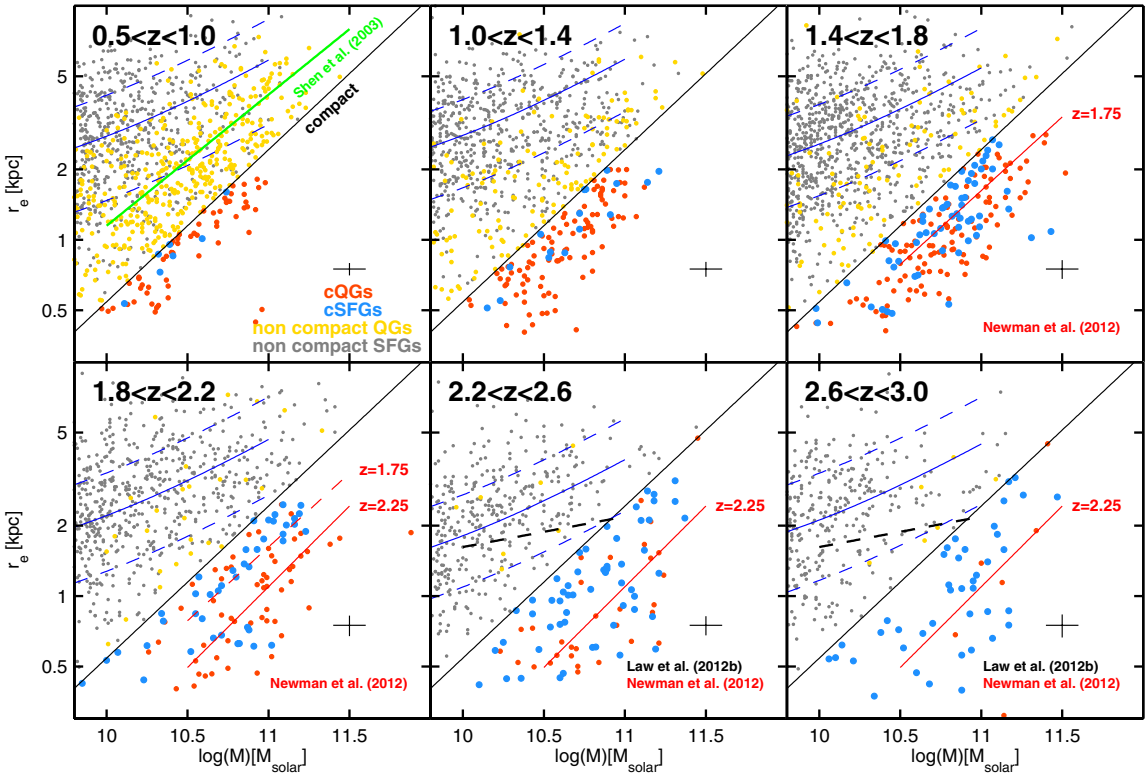

Figure 7. Evolution of the mass–size relation from $z = 3$ to $z = 0.5$ for galaxies above $M_\star > 10^{9.8}\ M_\odot$. The solid black line indicates the compactness selection criteria ($\Sigma_{1.5} = 10.3\ M_\odot\ \mathrm{kpc}^{-1.5}$). The blue and gray markers depict compact/non-compact SFGs and red and orange markers depict compact/non-compact quiescent galaxies. The solid blue line shows the best fit to the relation of Shen et al. (2003) for late-type galaxies at $z = 0$, leaving the normalization as a free parameter to characterize the redshift evolution. The 1σ scatter is shown with dashed lines. The green, red, and dashed-black lines indicate the mass–size relation for quiescent galaxies at $z = 0$ from Shen et al. (2003), at $z = 1.25$, 1.75, and 2.25 from Newman et al. (2012), and at $z = 2.0$–2.5 from Law et al. (2012).

(A color version of this figure is available in the online journal.)

a population of cSFGs at $z \gtrsim 2$ that are extremely uncommon at lower redshifts. Here we analyze the differential evolution of the mass–size relation for both populations, and the impact of the uncertainties in sizes and stellar masses on the robustness of the samples.

Figure 7 shows the evolution of the mass–size relation from $z = 3$ to $z = 0.5$ for the same galaxies shown in Figure 2. We characterize the size evolution for non-compact SFGs (the bulk of SFGs) by fitting their distribution to the relation of Shen et al. (2003) for late type galaxies ($n < 2$) leaving the normalization as the only free parameter. Based on this fit, we find an overall size evolution of a factor of $\sim$1.5 from $z = 3$ to 0.5 with a 1σ scatter of $\sim$0.2 dex. This is consistent with the size evolution estimated in Trujillo et al. (2007) or Buitrago et al. (2008), following a redshift dependence described by $r \propto (1+z)^{-0.8}$. Our results for QGs are also in good agreement with Newman et al. (2012 and references therein) for a size growth of a factor of $\sim$3 since $z = 2.5$. On average, QGs grow at a slightly faster rate than non-compact SFGs since $z \sim 3$. Their distribution in the mass–size plane suggests in fact that QGs experience a more accelerated size growth in the redshift range $z = 1$–2 as a result of a faster increment in the number of "normal"-sized (orange markers) ellipticals (see also Cassata et al. 2011). The lower number density of extended quiescent galaxies at $z \sim 2$ substantially reduces the overlap between the bulk of SFGs and QGs, creating an underdense region between the two, and at higher redshifts the overlap is restricted to a sub-population of compact SFGs (blue markers). These galaxies appear to follow more closely the steeper mass–size relation of QGs, and its evolution with redshift, than that of non-compact SFGs. Indeed, the distribution of cSFGs at each redshift bin seems to match very well the expected distribution for cQGs roughly one redshift bin later ($\sim$500 Myr), as we would expect if one is the progenitor population of the other.

We repeat this analysis in Figure 8 from the perspective of the scatter distribution, measured with respect to the best-fit mass–size relation for non-compact SFGs. At $z < 1$ the distribution for all galaxies (black line) can be approximated by a single peaked Gaussian with SFGs and QGs occupying the largest and smallest sizes, respectively. However, at higher redshifts the distribution is skewed toward smaller sizes, and by $z \sim 2$ the distribution is clearly bimodal, with QGs (red line) located in the secondary peak of smaller sizes. The bimodality is also present at $z > 2$ although the significance of the compact QG peak is reduced due to their rapidly decreasing number density at these redshifts (see Section 5). The distribution of SFGs (gray line) presents a similar skewing at $z > 1.5$ corresponding to the compact SFG population (blue line). The change in the shape of the distribution does not appear to be driven by uncertainties in r_e, or at least not any more than for QGs. On the contrary, the (1σ) scatter of the distribution for non-compact SFGs (shown in cyan) remains smaller than 0.20 dex up to $z = 3$, and the uncertainties for cSFGs are even smaller, as they are among the brightest galaxies of the sample. Their average magnitudes at $z = 1.8$ and $z = 2.2$ are $H = 22.7$ and 23.4 mag, more than two magnitudes brighter than the limiting magnitude, and the uncertainties in their effective radius are $\Delta\log(r_e) < 0.04$ dex (see also Appendix B2 of Wuyts et al.

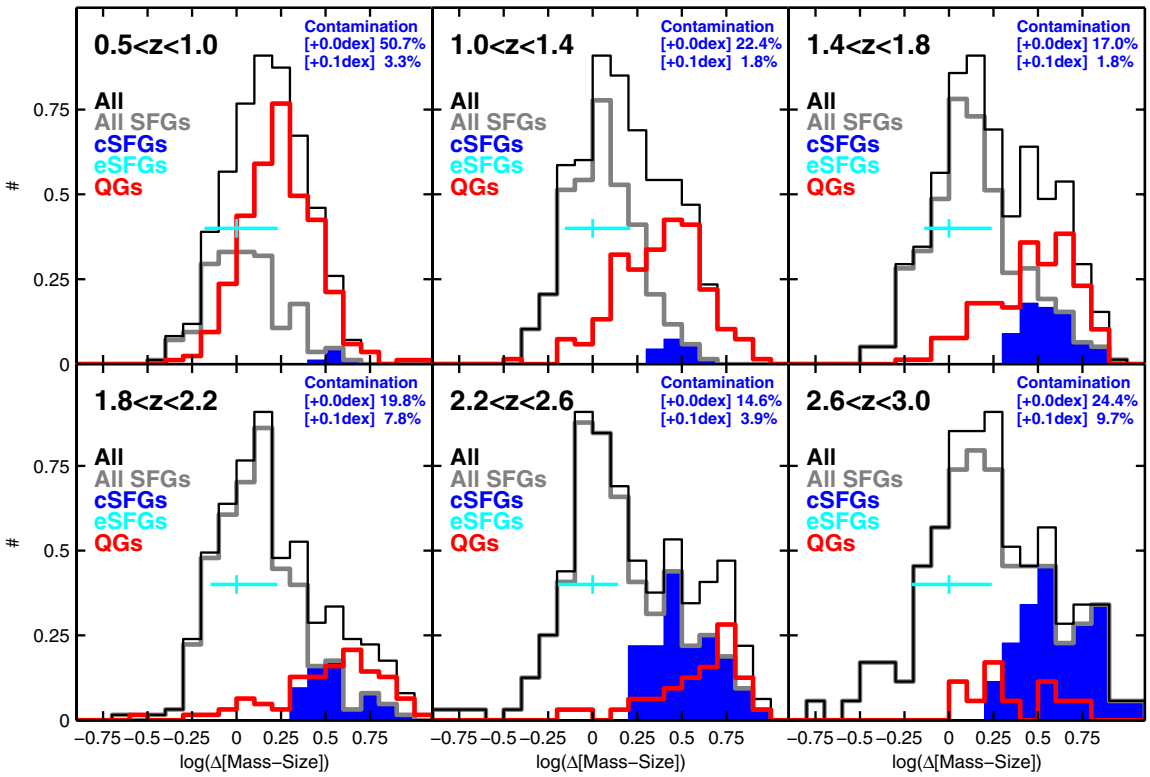

Figure 8. Distribution of the scatter with respect to the best-fitting mass–size relation for non-compact SFGs at each redshift bin from $0.5 < z < 3$. The color code indicates the different groups of galaxies. The cyan marker and lines show the median and 1σ width of the distribution for extended (non-compact) SFGs. The numbers on the upper right corner indicate the estimated fraction of contaminants that would be classified as cSFGs due to uncertainties in the size and stellar mass measurements at the $\Sigma_{1.5} = 10.3\ M_{\odot}\ \mathrm{kpc}^{-1.5}$ threshold and at $\Sigma_{1.5}$+0.1 dex. These fractions are estimated bootstrapping the uncertainties in stellar masses and effective radii.
(A color version of this figure is available in the online journal.)

(2011b) and van der Wel et al. (2013) for further analysis on the size uncertainties for these galaxies).

The values on the upper right corner of Figure 8 indicate the estimated fraction of non-compact SFGs scattered into the compact region due to uncertainties in r_e and stellar mass. In general, the contamination does not exceed a 20% at $z > 2$, and it lowers to less than 10% if we increase the selection threshold in $\Sigma_{1.5}$ by 0.1 dex, indicating that some cSFGs are clearly detected at $>5\sigma$ of the expected distribution for non-compact SFGs. This is mainly because the skewing, which can be as high as 0.6 dex, is more pronounced than the typical uncertainties in r_e (<0.04 dex) or the stellar mass (<0.2 dex). Note also that the scattered galaxies are not necessarily spurious. Some of them might in fact be moving into the compact region if, as advocated in Section 6, cSFGs are the result of highly dissipative processes that reduce the sizes of larger SFGs. In summary, cQGs and cSFGs not only present similar values of $\Sigma_{1.5}$ but also matching distributions on the mass–size plane (and similar Sérsic indices; Figure 3), which provides further evidence in favor of the proposed evolutionary scenario.

Finally, we note that if the distribution of SFGs in the mass–size plane is studied as a whole, without making any distinction for compact galaxies, the average size of the population at $z \gtrsim 2$ would be smaller, and the slope the mass–size relation would be flatter, as shown for example in Mosleh et al. (2011, 2012) or Law et al. (2012). The analysis of compact SFGs as a distinct sub-population is physically motivated by the widely demonstrated existence of cQGs at $z \sim 2$ (Szomoru et al. 2011; Cassata et al. 2011), whose most likely progenitors should shared some of their structural properties while still actively forming stars a $2 < z < 3$. Although our conclusions are based on the similarities between cSFGs and cQGs, and therefore are independent of this interpretation, the existence of a sub-population of SFGs following a steeper mass–size relation would have important implications on their formation mechanisms.

APPENDIX B

COLOR SELECTION OF STAR-FORMING AND QUIESCENT GALAXIES

As demonstrated in previous works, IR-based (mostly 24 μm) selection criteria are very efficient to discriminate SFGs and QGs down to relatively small values of the SFR $\sim 10\ M_{\odot}\ \mathrm{yr}^{-1}$ (Fontana et al. 2009; Santini et al. 2009; Wuyts et al. 2011b; Wang et al. 2012). Nonetheless, samples selected with this method do not overlap completely with those obtained with other SED based methods such color–color or age/τ (with τ being the timescale of the star formation burst) criteria. In addition, IR detections are susceptible of contamination in the presence of an additional dust heating source, such as AGN activity (Daddi et al. 2007). In this work we used X-ray data to identify the most luminous AGNs. For these galaxies the sSFR was computed from the UV luminosity corrected for extinction instead of from 24 μm based SFR (Section 4.1). We complemented this analysis with a search for IRAC power-law galaxies (PLG) that may host obscured AGNs undetected in the X-ray data (Donley et al. 2008). However, we do not identify new AGNs (i.e., not detected in the X-ray data) among cSFGs

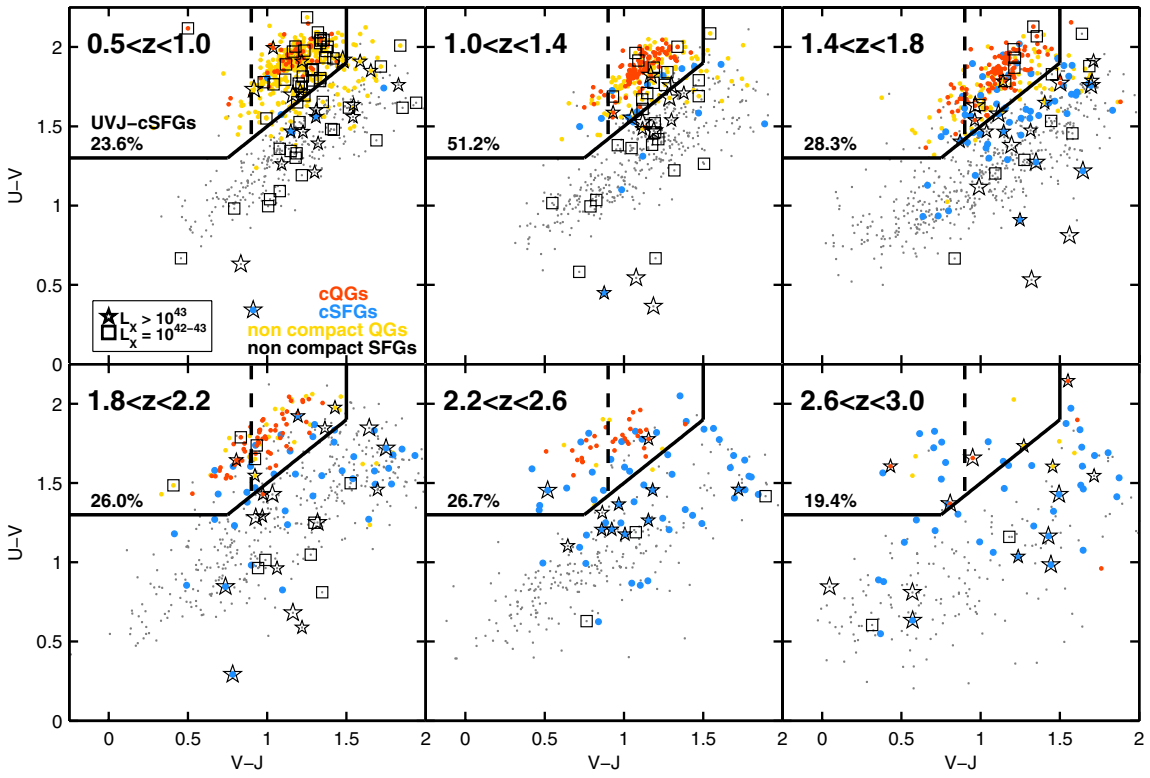

Figure 9. *UVJ* diagram from $z = 3$ to $z = 0.5$ for galaxies above $M_\star > 10^{9.8}\ M_\odot$. The color code is the same as in Figure 7. The percentage on the top-left corner indicates the fraction of cSFGs that lie on the quiescent locus of the *UVJ* selection criteria. As shown in previous works (e.g., Brammer et al. 2009), we find that some IR-selected star-forming galaxies (∼25% of the cSFGs) are classified as quiescent attending to their rest-frame colors. We advocate that these are likely SFGs in the final stages of the star formation burst, and probably starting to quench. Some of these galaxies occupy a region of the *UVJ* diagram (left of the black dashed line) where recently quenched (post-starburst) galaxies have been identified (Whitaker et al. 2012a).

(A color version of this figure is available in the online journal.)

using this criterion. Therefore we do not expect a significant contamination on the IR-based SFRs of the remaining cSFGs.

In order to compare the sSFR selected sample with other criteria, Figure 9 presents the $U - V$ versus $V - J$ (hereafter *UVJ*) rest-frame colors for the same galaxies shown in Figure 2. The *UVJ* criterion is alternative method to discriminate dusty SFGs and QGs using the $V - J$ color as a proxy for dust attenuation (Wuyts et al. 2007; Brammer et al. 2009). In essence, this method relies on the sensitivity of the rest-frame V band to the effects of dust attenuation (Whitaker et al. 2011). Our photometric catalog counts with extensive NIR data (J, H, K, and IRAC), some of which from *HST*, accurately probing this spectral region up to $z \sim 3$. The cSFGs identified with the sSFR criteria are shown in blue, and the percentage of these that are found in the quiescent region of the *UVJ* diagram is indicated in the upper-left corner. In agreement with previous results, we find that the IR-based selection and the *UVJ* criterion are largely consistent (e.g., Brammer et al. 2011; Bell et al. 2012). However, ∼25% of the IR-selected SFGs (i.e., 24 μm detected galaxies) are found in the *UVJ* quiescent region. The causes of this apparent discrepancy are not entirely clear. Uncertainties in the photometric redshifts and rest-frame colors could scatter sources into different regions. Nevertheless, multiple 24 μm detected galaxies are found in the quiescent region whereas very few MIPS undetected galaxies (red and orange markers) are found outside the *UVJ* quiescent region at $z > 1.5$. AGN contamination is another possible cause. However, we do not find a high fraction of X-ray detections (nor obscured IRAC-PLGs) among the cSFGs in the *UVJ* quiescent region. Although at the depth of the X-ray data we could be missing some low-luminosity (low accretion rate) AGNs in quiescent galaxies, these would not dominate the emission at short, 8–10 μm, IR wavelengths (e.g., Trump et al. 2011), and even at intermediate X-ray luminosities, recent *Herschel* results suggest that the AGN rarely dominates the total IR luminosity, i.e., these are typically composite galaxies with an star-forming component (Elbaz et al. 2011; Rosario et al. 2012). In summary, while we cannot completely rule out an AGN component on these galaxies, we expect that at least part of the observed IR emission will be originated by ongoing star formation.

In this regard, an alternative interpretation could be a difference in the *quiescence* of the galaxies selected by the sSFR and the *UVJ* criterion. As shown in Williams et al. (2009) and Whitaker et al. (2012a), there is a inside-out gradient toward higher sSFRs (and younger ages) for galaxies in the *UVJ* quiescent locus. Indeed, many cSFGs at $z > 2$ lie in a region of the diagram ($V - J < 0.9$) which, according to Whitaker et al. (2012a), is associated with recently quenched (post-starburst) galaxies. This would be consistent with the scenario in which cSFGs are a heterogeneous population consisting of galaxies in different stages of the starburst to quiescent path, rapidly consuming their gas reservoirs in a nuclear starburst and eventually quenching in timescales of less than 1 Gyr.

REFERENCES

Aird, J., Nandra, K., Laird, E. S., et al. 2010, MNRAS, 401, 2531
Baldry, I. K., Glazebrook, K., Brinkmann, J., et al. 2004, ApJ, 600, 681

Barro, G., Pérez-González, P. G., Gallego, J., et al. 2011, ApJS, 193, 30
Bell, E. F. 2008, ApJ, 682, 355
Bell, E. F., Papovich, C., Wolf, C., et al. 2005, ApJ, 625, 23
Bell, E. F., van der Wel, A., Papovich, C., et al. 2012, ApJ, 753, 167
Bell, E. F., Wolf, C., Meisenheimer, K., et al. 2004, ApJ, 608, 752
Bertin, E., & Arnouts, S. 1996, A&AS, 117, 393
Bezanson, R., van Dokkum, P., & Franx, M. 2012, ApJ, 760, 62
Bezanson, R., van Dokkum, P. G., Tal, T., et al. 2009, ApJ, 697, 1290
Birnboim, Y., & Dekel, A. 2003, MNRAS, 345, 349
Brammer, G. B., van Dokkum, P. G., & Coppi, P. 2008, ApJ, 686, 1503
Brammer, G. B., Whitaker, K. E., van Dokkum, P. G., et al. 2009, ApJL, 706, L173
Brammer, G. B., Whitaker, K. E., van Dokkum, P. G., et al. 2011, ApJ, 739, 24
Bruce, V. A., Dunlop, J. S., Cirasuolo, M., et al. 2012, MNRAS, 427, 1666
Bruzual, G., & Charlot, S. 2003, MNRAS, 344, 1000
Buitrago, F., Trujillo, I., Conselice, C. J., & Häußler, B. 2013, MNRAS, 428, 1460
Buitrago, F., Trujillo, I., Conselice, C. J., et al. 2008, ApJL, 687, L61
Bundy, K., Scarlata, C., Carollo, C. M., et al. 2010, ApJ, 719, 1969
Calzetti, D., Armus, L., Bohlin, R. C., et al. 2000, ApJ, 533, 682
Cassata, P., Giavalisco, M., Guo, Y., et al. 2011, ApJ, 743, 96
Cattaneo, A., Dekel, A., Devriendt, J., Guiderdoni, B., & Blaizot, J. 2006, MNRAS, 370, 1651
Cava, A., Rodighiero, G., Pérez-Fournon, I., et al. 2010, MNRAS, 409, L19
Ceverino, D., Dekel, A., & Bournaud, F. 2010, MNRAS, 404, 2151
Chabrier, G. 2003, PASP, 115, 763
Chary, R., & Elbaz, D. 2001, ApJ, 556, 562
Cheung, E., Faber, S. M., Koo, D. C., et al. 2012, ApJ, 760, 131
Ciotti, L., Ostriker, J. P., & Proga, D. 2009, ApJ, 699, 89
Cisternas, M., Jahnke, K., Inskip, K. J., et al. 2011, ApJ, 726, 57
Covington, M., Dekel, A., Cox, T. J., Jonsson, P., & Primack, J. R. 2008, MNRAS, 384, 94
Covington, M. D., Primack, J. R., Porter, L. A., et al. 2011, MNRAS, 415, 3135
Croton, D. J. 2009, MNRAS, 394, 1109
Daddi, E., Alexander, D. M., Dickinson, M., et al. 2007, ApJ, 670, 173
Daddi, E., Bournaud, F., Walter, F., et al. 2010a, ApJ, 713, 686
Daddi, E., Elbaz, D., Walter, F., et al. 2010b, ApJL, 714, L118
Damjanov, I., McCarthy, P. J., Abraham, R. G., et al. 2009, ApJ, 695, 101
Dekel, A., Birnboim, Y., Engel, G., et al. 2009a, Natur, 457, 451
Dekel, A., Sari, R., & Ceverino, D. 2009b, ApJ, 703, 785
Di Matteo, T., Springel, V., & Hernquist, L. 2005, Natur, 433, 604
Donley, J. L., Rieke, G. H., Pérez-González, P. G., & Barro, G. 2008, ApJ, 687, 111
Elbaz, D., Dickinson, M., Hwang, H. S., et al. 2011, A&A, 533, A119
Faber, S. M., Willmer, C. N. A., Wolf, C., et al. 2007, ApJ, 665, 265
Ferrarese, L., & Merritt, D. 2000, ApJL, 539, L9
Fontana, A., Santini, P., Grazian, A., et al. 2009, A&A, 501, 15
Förster Schreiber, N. M., Genzel, R., Bouché, N., et al. 2009, ApJ, 706, 1364
Franx, M., van Dokkum, P. G., Schreiber, N. M. F., et al. 2008, ApJ, 688, 770
Gabor, J. M., & Davé, R. 2012, MNRAS, 427, 1816
Geach, J. E., Smail, I., Moran, S. M., et al. 2011, ApJL, 730, L19
Genzel, R., Tacconi, L. J., Gracia-Carpio, J., et al. 2010, MNRAS, 407, 2091
Giavalisco, M., Ferguson, H. C., Koekemoer, A. M., et al. 2004, ApJL, 600, L93
Governato, F., Brook, C. B., Brooks, A. M., et al. 2009, MNRAS, 398, 312
Graham, A. W., Driver, S. P., Petrosian, V., et al. 2005, AJ, 130, 1535
Grogin, N. A., Kocevski, D. D., Faber, S. M., et al. 2011, ApJS, 197, 35
Guo, Y., Giavalisco, M., Cassata, P., et al. 2011, ApJ, 735, 18
Hilz, M., Naab, T., Ostriker, J. P., et al. 2012, MNRAS, 425, 3119
Hopkins, P. F., Cox, T. J., Younger, J. D., & Hernquist, L. 2009a, ApJ, 691, 1168
Hopkins, P. F., Hernquist, L., Cox, T. J., & Kereš, D. 2008, ApJS, 175, 356
Hopkins, P. F., Hernquist, L., Cox, T. J., Keres, D., & Wuyts, S. 2009b, ApJ, 691, 1424
Hopkins, P. F., Hernquist, L., Cox, T. J., et al. 2006, ApJS, 163, 1
Ilbert, O., Salvato, M., Le Floc'h, E., et al. 2010, ApJ, 709, 644
Karim, A., Schinnerer, E., Martínez-Sansigre, A., et al. 2011, ApJ, 730, 61
Kartaltepe, J. S., Dickinson, M., Alexander, D. M., et al. 2012, ApJ, 757, 23
Kauffmann, G., Heckman, T. M., White, S. D. M., et al. 2003, MNRAS, 341, 54
Kaviraj, S., Cohen, S., Ellis, R. S., et al. 2013, MNRAS, 428, 925
Kennicutt, R. C., Jr. 1998, ARA&A, 36, 189
Kereš, D., Katz, N., Weinberg, D. H., & Davé, R. 2005, MNRAS, 363, 2
Kocevski, D. D., Faber, S. M., Mozena, M., et al. 2012, ApJ, 744, 148
Koekemoer, A. M., Faber, S. M., Ferguson, H. C., et al. 2011, ApJS, 197, 36
Kormendy, J., & Kennicutt, R. C., Jr. 2004, ARA&A, 42, 603
Kriek, M., van Dokkum, P. G., Franx, M., Illingworth, G. D., & Magee, D. K. 2009a, ApJL, 705, L71
Kriek, M., van Dokkum, P. G., Labbé, I., et al. 2009b, ApJ, 700, 221
Kron, R. G. 1980, ApJS, 43, 305
Laidler, V. G., Grogin, N., Clubb, K., et al. 2006, in ASP Conf. Ser. 351, Astronomical Data Analysis Software and Systems XV, ed. C. Gabriel, C. Arviset, D. Ponz, & S. Enrique (San Francisco, CA: ASP), 228
Law, D. R., Steidel, C. C., Shapley, A. E., et al. 2012, ApJ, 745, 85
Lotz, J. M., Jonsson, P., Cox, T. J., et al. 2011, ApJ, 742, 103
Marchesini, D., Whitaker, K. E., Brammer, G., et al. 2010, ApJ, 725, 1277
Martig, M., Bournaud, F., Teyssier, R., & Dekel, A. 2009, ApJ, 707, 250
Masters, K. L., Mosleh, M., Romer, A. K., et al. 2010, MNRAS, 405, 783
Mendez, A. J., Coil, A. L., Lotz, J., et al. 2011, ApJ, 736, 110
Mosleh, M., Williams, R. J., Franx, M., & Kriek, M. 2011, ApJ, 727, 5
Mosleh, M., Williams, R. J., Franx, M., et al. 2012, ApJL, 756, L12
Mullaney, J. R., Daddi, E., Béthermin, M., et al. 2012, ApJL, 753, L30
Naab, T., Johansson, P. H., & Ostriker, J. P. 2009, ApJL, 699, L178
Naab, T., Johansson, P. H., Ostriker, J. P., & Efstathiou, G. 2007, ApJ, 658, 710
Naab, T., & Trujillo, I. 2006, MNRAS, 369, 625
Newman, A. B., Ellis, R. S., Bundy, K., & Treu, T. 2012, ApJ, 746, 162
Olsen, K. P., Rasmussen, J., Toft, S., & Zirm, A. W. 2013, ApJ, 764, 4
Oser, L., Ostriker, J. P., Naab, T., Johansson, P. H., & Burkert, A. 2010, ApJ, 725, 2312
Patel, S. G., van Dokkum, P. G., Franx, M., et al. 2012, arXiv:1208.0341
Peng, C. Y., Ho, L. C., Impey, C. D., & Rix, H.-W. 2002, AJ, 124, 266
Pérez-González, P. G., Rieke, G. H., Villar, V., et al. 2008, ApJ, 675, 234
Pierce, C. M., Lotz, J. M., Primack, J. R., et al. 2010, MNRAS, 405, 718
Robertson, B., Bullock, J. S., Cox, T. J., et al. 2006, ApJ, 645, 986
Rodighiero, G., Daddi, E., Baronchelli, I., et al. 2011, ApJL, 739, L40
Rosario, D. J., Santini, P., Lutz, D., et al. 2012, A&A, 545A, 45
Salvato, M., Hasinger, G., Ilbert, O., et al. 2009, ApJ, 690, 1250
Salvato, M., Ilbert, O., Hasinger, G., et al. 2011, ApJ, 742, 61
Santini, P., Fontana, A., Grazian, A., et al. 2009, A&A, 504, 751
Santini, P., Rosario, D. J., Shao, L., et al. 2012, A&A, 540, A109
Saracco, P., Longhetti, M., & Gargiulo, A. 2010, MNRAS, 408, L21
Sargent, M. T., Béthermin, M., Daddi, E., & Elbaz, D. 2012, ApJL, 747, L31
Scarlata, C., Carollo, C. M., Lilly, S. J., et al. 2007, ApJS, 172, 494
Shen, S., Mo, H. J., White, S. D. M., et al. 2003, MNRAS, 343, 978
Simmons, B. D., & Urry, C. M. 2008, ApJ, 683, 644
Springel, V., & Hernquist, L. 2005, ApJL, 622, L9
Springel, V., White, S. D. M., Jenkins, A., et al. 2005, Natur, 435, 629
Szomoru, D., Franx, M., Bouwens, R. J., et al. 2011, ApJL, 735, L22
Szomoru, D., Franx, M., & van Dokkum, P. G. 2012, ApJ, 749, 121
Tacconi, L. J., Genzel, R., Neri, R., et al. 2010, Natur, 463, 781
Toft, S., van Dokkum, P., Franx, M., et al. 2007, ApJ, 671, 285
Trujillo, I., Conselice, C. J., Bundy, K., et al. 2007, MNRAS, 382, 109
Trump, J. R., Impey, C. D., Kelly, B. C., et al. 2011, ApJ, 733, 60
Ueda, Y., Watson, M. G., Stewart, I. M., et al. 2008, ApJS, 179, 124
van der Wel, A., Bell, E. F., Häussler, B., et al. 2013, ApJS, 203, 24
van der Wel, A., Rix, H.-W., Wuyts, S., et al. 2011, ApJ, 730, 38
van Dokkum, P. G., Whitaker, K. E., Brammer, G., et al. 2010, ApJ, 709, 1018
Wake, D. A., van Dokkum, P. G., & Franx, M. 2012, ApJL, 751, L44
Wang, T., Huang, J.-S., Faber, S. M., et al. 2012, ApJ, 752, 134
Whitaker, K. E., M., Kriek, van Dokkum, P. G., et al. 2012a, ApJ, 745, 179
Whitaker, K. E., Labbé, I., van Dokkum, P. G., et al. 2011, ApJ, 735, 86
Whitaker, K. E., van Dokkum, P. G., Brammer, G., & Franx, M. 2012b, ApJL, 754, L29
Williams, R. J., Quadri, R. F., & Franx, M. 2011, ApJL, 738, L25
Williams, R. J., Quadri, R. F., Franx, M., van Dokkum, P., & Labbé, I. 2009, ApJ, 691, 1879
Williams, R. J., Quadri, R. F., Franx, M., et al. 2010, ApJ, 713, 738
Wuyts, S., Cox, T. J., Hayward, C. C., et al. 2010, ApJ, 722, 1666
Wuyts, S., Förster Schreiber, N. M., Lutz, D., et al. 2011a, ApJ, 738, 106
Wuyts, S., Förster Schreiber, N. M., van der Wel, A., et al. 2011b, ApJ, 742, 96
Wuyts, S., Labbé, I., Franx, M., et al. 2007, ApJ, 655, 51
Xue, Y. Q., Luo, B., Brandt, W. N., et al. 2011, ApJS, 195, 10